Numerical thermal evaluation of laminated binary microencapsulated phase change material drywall systems

Weiguang Su[1,a], Jo Darkwa[2], Georgios Kokogiannakis[3]

1. School of Mechanical & Automotive Engineering, Qilu University of Technology(Shandong Academy of Sciences), No.3501 Daxue Road, Changqing District, 250353, Jinan, China
2. Faculty of Engineering, University of Nottingham, Room B20 Lenton Firs, University Park, Nottingham, NG7 2RD, UK
3. Sustainable Buildings Research Centre, University of Wollongong, Building 237, Innovation Campus, Squires Way, Fairy Meadow NSW 2519, Australia

Acknowledgements: The authors are thankful to Natural Science Foundation of Shandong Province (No. ZR2017LEE017) and the Youth Doctoral Cooperation Project of Qilu University of Technology (No. 2018BSHZ0023).

[a] Corresponding author. E-mail address: wgsuper@hotmail.com/weiguang.su@qlu.edu.cn

Numerical thermal evaluation of laminated binary microencapsulated phase change material drywall systems

Abstract: Microencapsulated phase change materials (MEPCMs) have the potential for energy storage applications in buildings. However, current MEPCMs are limited by their singular phase change transitional temperatures and are therefore unable to satisfy all year seasonal energy storage applications. This study was focused on numerically assessing the energy saving potential of a binary MEPCM drywall system which is capable of operating within two different phase change transitional temperature ranges. In this study, Ansys Fluent and the ESP-r simulation tools were employed because Fluent could offer a detailed quantification of the temperature changes within the composite drywall system and ESP-r has the capability of thermal modelling of phase change materials at whole building scale by using annual weather data as boundary conditions. The Fluent simulation results demonstrated that the thermal energy charge time and thermal energy charge/discharge amount of the binary MEPCM drywall were significantly increased when the MEPCM thickness increased from 1 mm to 5 mm, and the 5 mm thick layer had adequate capacity to balance the thermal energy during day and night. The ESP-r results showed that for the hot period in Hangzhou (China), the 5 mm thick binary MEPCM drywall was able to achieve a maximum peak air temperature reduction of about 6.7℃ and to increase the number of hours the indoor air temperatures were within the 21-28°C range by about 12% in

comparison with other drywalls. Experimental evaluation is therefore being recommended to verify the full practical potential of MEPCMs with two phase change temperature ranges.

Keywords: binary microencapsulated phase change material drywall, thermal performance, energy storage, whole building simulation of MEPCMs, two phase change temperature ranges.

Highlights:

- The 5 mm binary MEPCM drywall was able to balance thermal energy for day and night.
- The binary MEPCM drywall had better performance than the single MEPCM.
- The binary MEPCM drywall was able to reduce the peak indoor temperature by 6.7°C.
- Indoor temperatures were improved by 12% with the 5 mm binary MEPCM drywall.

Nomenclature

C_p	Specific heat (kJ/kg·K)
g	Heat generation rate (W/m^3)
H_P	Total enthalpy of the MEPCM (kJ/kg)

ΔH	Latent heat enthalpy (kJ/kg)
h	Sensible heat enthalpy (kJ/kg)
h_f	Convection heat transfer coefficient (W/m^{2}K)
k	Thermal conductivity (W/mK)
L	Latent heat enthalpy of MEPCM (kJ/kg)
$\vec{n}$	Outward drawn normal unit vector
q	Heat flux (W/m^2)
T	Temperature (°C)
$\bar{T}$	Average temperature (°C)
t	Time (s)
V	Control volume (m^3)
β	Liquid fraction
ρ	Density (kg/m^3)

Subscripts:

a: Air

e: Effective

l: Liquid

m: Melting

s: Solid

w: The wall surface exposed to the air

1 Introduction

Currently the building sector consumes more than 30% of total global final energy supply (Berardi 2017), and recent research has focused on reducing the energy demand of buildings by applying for example thermal storage innovations such as phase change materials (PCMs). Microencapsulated phase change materials (MEPCMs) have been recognized as potential energy storage materials which could be used for reducing energy consumption and carbon emissions in buildings by improving the indoor temperatures and therefore reducing the risk for overheating in summer (Su 2015). For instance, the reviews carried out by Konuklu *et al*. (2015), Alva *et al*. (2017) and Jamekhorshid *et al*. (2017) showed that MEPCMs could be incorporated into various construction materials (i.e. concrete, mortar, plaster, wood, plastics etc.) to enhance their thermal capacity and performance. This was supported by an experimental investigation (Kuznik and Virgone 2009) conducted with copolymer composite MEPCM wallboard, which resulted into a room air temperature reduction up to 4.2°C. Another investigation was done by Berthou *et al*. (2015) who showed that a novel translucent full-scale passive solar MEPCM wall could provide a significant improvement of indoor temperatures for cold sunny climates. Darkwa *et al*. (2012) also developed a non-deform MEPCM for thermal energy storage applications and was later evaluated by Zhou *et al*. (2015) in a model room where it achieved a maximum temperature reduction of 5°C. Young *et al*. (2018) combined MEPCM with

plain mortar and achieved a significant reduction in the amplitude of the indoor temperature. Lee *et al*. (2018) enhanced the thermal performance of a residential building with the addition of PCM. Their results report a daily average peak heat flux reduction for the walls of up to 25.4%. A theoretical evaluation of an integrated PCM insulation layer by Fateh *et al*. (2018) showed that up to about 75% of heating load could be saved, while Alam *et al*. (2014) demonstrated that an integrated MEPCM building envelope could achieve about 23% of energy savings.

However, the potential of all these MEPCMs to improve indoor temperatures is limited by their singular transitional phase change temperatures and they are therefore unable to cover multiple seasons such as summer and winters with high diurnal temperature variations. This has led to various studies such as the one by Thiele *et al*. (2015) where they concluded that the best condition for combining building materials and MEPCMs is in a situation where the yearly outdoor temperature fluctuates around the desired indoor air temperature. Other researchers (Tokuç 2015, Zhu 2015, Zhu 2016) have also suggested mixing two or more MEPCMs with construction materials to overcome the seasonal storage limitations. Past investigations by Darkwa and Kim (2004) did however establish that randomly mixing MEPCMs with building materials affected their thermal response factor, hence the concept of laminating MEPCMs was introduced. To this end, instead of randomly mixing MEPCMs and single MEPCM as latent heat thermal energy storage materials, this study proposes a binary MEPCM drywall system which is capable of operating within two different phase change

transition temperature ranges. Moreover, this study intends to evaluate the thermal performance of a laminated binary MEPCM drywall system through numerical simulation and identify the indoor temperature profiles compared with single MEPCM drywall.

In this research Hangzhou, China (longitude 120°12 east and at latitude 30°16 north) was selected as an example for the application of this type of laminated binary MEPCM drywall. Hangzhou has a typical climate of hot summer and cold winter (Mi 2016). The weather records of Hangzhou (Yi 2005) showed that the yearly ambient temperature typically ranges between -3°C and 37°C and that the ambient temperature in summer will most likely lead to overheating indoors. Mitigating thermal discomfort in summer is an interesting application for MEPCMs and it was the main application that this paper focused on.

2 Methodology

Due to the binary and dynamic nature of the proposed system, two types of computer software programs (Ansys Fluent and ESP-r) were employed for the investigation. Ansys Fluent can define the ambient temperature profile by user-defined functions (UDFs) and is capable of offering more details in monitoring the temperature change within the composite drywall system. On the other hand, ESP-r as a dynamic whole building energy simulation tool (ESP-r 2015), has the capability of thermal modelling of phase change materials in buildings and also importing historical weather data as

boundary conditions. In the initial stage, the Fluent software was used to determine the charging/discharging abilities of the proposed binary MEPCM drywall and establish a suitable binary MEPCM drywall thickness before the whole building simulation exercise was carried out with ESP-r. The thermal comfort range and maximum environmental temperature of Hangzhou (Yi 2005) were chosen as 21-28°C and 37°C, respectively.

2.1 MEPCMs drywall thickness

2.1.1 Physical model

Based on previous MEPCM fabrication processes, thermophysical data of MEPCM samples (Darkwa and Su 2017, Su 2017, Su 2017, Su 2018, Su 2019), and typical phase change temperature range of MEPCMs for cooling applications in buildings (Du 2018), two types of MEPCMs, i.e. encapsulated n-octadecane (MEPCM-oct) and n-eicosane (MEPCM-eic), with phase change temperatures of 23.55°C and 34.99°C respectively (see Tab. 1) were selected as the base materials for the laminated binary MEPCM drywall. However, it should be noted that using the same binary MEPCM drywall may not suit buildings in different climates and that the focus period of this study is summer because these specific materials would not be fully utilised during the winter (i.e. the specific MEPCMs would be mostly in solid state).

As shown in Fig.1, the laminated binary MEPCM drywall consists of two layers that

have equal thicknesses and equal amounts (50 vol% / 50 vol%) of MEPCM-oct and MEPCM-eic. The MEPCM-oct was placed on the internal side of the room since its melting temperature falls within typically acceptable temperature ranges from the thermal comfort point of view. More specifically, MEPCM-oct will charge/discharge latent heat when the indoor temperature is above/below 23.55 °C and will most likely have shorter thermal response time to the variations of the indoor temperature than the MEPCM-eic layer. To assess the thermal response of the laminated binary MEPCM drywall system, different drywall thicknesses of 1 (0.5+0.5) mm, 2 (1+1) mm and 5 (2.5+2.5) mm were considered and simulated with the Ansys Fluent software. The external walls include the following three layers: wood, fiberglass and plaster board, which is a lightweight construction that was available in the constructions database of the 'BESTEST ' test cells (Judkoff and Neymark 1995), as shown in Tab.2.

2.1.2 Heat transfer model in Ansys Fluent

Since there is no internal heat generation and mass transfer, the governing equation during solidification/melting process for the latent energy storage layer can be expressed as (Ansys 2015):

$$\frac{\partial}{\partial t}\left(\rho H_P\right) = \nabla \bullet \left(k \nabla T\right) \tag{1}$$

Where T is temperature, ρ is density, H_P is the total enthalpy, k is thermal

conductivity. The total enthalpy of the MEPCM is computed as the sum of the specific heat enthalpy of MEPCM (h) (Ansys 2015) and the latent heat enthalpy of MEPCM (ΔH) (Ansys 2015):

$$H_P = h + \Delta H \tag{2}$$

Where:

$$h = \int_{T_0}^{T} C_p dT \tag{3}$$

$$\Delta H = \beta L \tag{4}$$

C_p is the effective specific heat capacity, β is the liquid fraction, and L is latent heat enthalpy of MEPCM. The liquid fraction can also be calculated with the equation below as:

$$\beta = \begin{cases} 0 & (T < T_m) \\ \dfrac{T - T_m}{T_l - T_m} & (T_m < T < T_l) \\ 1 & (T > T_l) \end{cases} \tag{5}$$

Where T_m is the melting point temperature of MEPCM and T_l is the temperature at which MEPCM is fully melted.

On the external non-PCM wall layers (i.e. plaster, fiberglass and wood in Fig.1) there was no solidification/melting process, no internal heat generation and mass transfer, and therefore the governing equation can be simplified based on Eq.1 as:

$$\frac{\partial}{\partial t}(\rho h) = \nabla \bullet (k \nabla T) \tag{6}$$

The convective heat transfer between the exposed surface of wallboards (i.e. the external drywall surface boundary layer and the exposed wood surface towards the outside in Fig.1) and the air can be calculated from the following equation:

$$q = h_f (T_w - T_a) \tag{7}$$

Where q is the heat flux, h_f is convection heat transfer coefficient, T_w is the temperature of the wall surface layer exposed to the air and T_a is the air temperature.

2.1.3 Boundary conditions

To simplify the heat transfer process of the binary MEPCM drywall, the following assumptions were made: 1) The boundary conditions for the exposed surface of the drywall towards the indoor space (external drywall surface boundary layer in Fig.1) and for the exposed wood surface towards the outdoors were considered as natural convection; 2) The ambient outdoor temperature change was based on the environmental conditions for Hangzhou (Yi 2005) from May to October with average ambient temperature of 24.2°C, maximum ambient temperature of 37°C and average daily temperature difference of 10°C. The variations in the external ambient temperatures in 24 hours (86400 seconds) were described as sinusoidal by using Equations 8 & 9 with user-defined-functions (UDF) in Fluent. The low temperature cycle for normal days which is between 20°C and 30°C (293.15K - 303.15K) was

represented by Eq.8, while the high temperature cycle for hot days for temperatures between 30°C and 40°C (303.15K -313.15K) was expressed with Eq.9:

$$T = 5\sin\left(\frac{2\pi}{86400} * t - \frac{\pi}{2}\right) + 298.15 \quad (8)$$

$$T = 5\sin\left(\frac{2\pi}{86400} * t - \frac{\pi}{2}\right) + 308.15 \quad (9)$$

3) The indoor spaces were considered free-floating zones and the initial temperature was set as 20°C and 30°C for the low and high temperature cycle, respectively. The indoor air temperature gradient was limited at a distance of 10 cm from the external drywall surface boundary layer due to small indoor temperature difference. Therefore, the indoor temperature changes can be calculated by convection heat transfer between the external drywall surface boundary layer and the indoor air by using Eq.7. Moreover, the drywall temperature calculations took into account the conductive heat exchanges between the various wallboard layers (Eq.6) and the convective heat transfer (Eq.7) during low and high temperature cycles.

2.2 Whole model building simulation

2.2.1 Building model

Fig. 2 shows a pictorial view of a building model with a 20 m^2 floor area (5m x 4m) and 2.7m floor-to-ceiling height. The model includes a south facing door (1.2m x

2.1m) and a north located window (2m x 1m). The building is assumed to be made of a lightweight construction based on construction data from the 'BESTEST ' test cells (Judkoff and Neymark 1995) but the inside walls and the roof are laminated with a laminated binary MEPCM drywall. For the purpose of analysis of thermal performance, other cases covering walls/roof without MEPCM (see Tab.2 and Tab.3) and walls/roof with a laminated MEPCM-oct or MEPCM-eic layer that have the same thickness as the binary MEPCM drywall (see Tab.1) were simulated and compared with that of the binary MEPCM model.

The thermal performance of the building was simulated over a six-month period (May to October) with the ESP-r software by using weather data for Hangzhou, China (Yi 2005). The heat transfer process in a composite MEPCM drywall layer is more complex than in a standard wall construction due to the phase change process. The following assumptions were therefore made for the simulations:

a) All internal heat gain sources and furniture in the building were not considered.

b) The weather data was based on Chinese Standard Weather Data (CSWD) of the year 2005 (Yi 2005).

c) The MEPCM layers were treated as a whole body with uniform equivalent physical and thermal properties.

d) The heat transfer process was considered as one-dimensional for relatively thin MEPCM layers.

2.2.2 Mathematical modelling with ESP-r

In ESP-r, the differential equation of transient heat conduction with variable thermo-physical properties is given by Eq.10 (Heim and Clarke 2004):

$$\frac{\partial}{\partial t}\left(\rho(T)H_P(T)\right)=\nabla\bullet\left[k(T)\nabla T(\vec{r},t)\right]+g(\vec{r},t) \tag{10}$$

Where T is temperature, ρ is density, H_P is the total enthalpy, k is thermal conductivity and g is the heat generation rate.

When $\frac{\partial\rho}{\partial t}\approx 0$, $g(\vec{r},t)=0$ and $\frac{\partial H_P}{\partial t}=\frac{\partial H_P}{\partial T}\frac{\partial T}{\partial t}=C_{\mathrm{p,e}}(T)\frac{\partial T}{\partial t}$, Eq. (10) becomes:

$$\rho(T)\mathsf{C}_{P,e}\frac{\partial T}{\partial t}=\nabla\bullet\left[k(T)\nabla T(\vec{r},t)\right] \tag{11}$$

Where $\mathsf{C}_{P,e}$ is the effective specific heat capacity (Almeida 2010). During the phase change temperature period and as defined by Eq. (11), the Goodman transform can be used to remove the temperature dependent $\mathsf{C}_{P,e}$ outside the differential operator by defining a new dependent variable:

$$v=\int_{C_{Ps}}^{C_{Pl}}C_{P,e}(T)\,dT \tag{12}$$

$$C_{p,e} = \begin{cases} C_{p_s} & T < T_m \\ C_{p_s} + \dfrac{L}{T_l - T_m} & T_m < T < T_l \\ C_{p_l} & T > T_l \end{cases} \quad (13)$$

Where, C_{p_s} and C_{p_l} are the specific heat in solid and liquid phase respectively. Thus Eq. (11) becomes:

$$\rho(T) C_{p_e}(T) \frac{\partial T}{\partial v} \frac{\partial v}{\partial t} = \nabla \bullet \left[k(T) \frac{\partial T}{\partial v} \rho(T) \nabla v \right] \quad (14)$$

The ESP-r control volume approach was adapted to describe the physical elements of the PCM model using ESP-r's zones and networks elements (Heim and Clarke 2004). The control volume formulation was obtained by integrating the associated partial differential Eq. (11) over a small polyhedron control volume (*V)*, and thus it becomes:

$$\rho(\bar{T}) C_{p_e}(\bar{T}) V(\bar{T}) \frac{\partial \bar{T}}{\partial t} = -k(T) \frac{\partial T}{\partial \vec{n}} \quad (15)$$

Where $\bar{T}$ is the average temperature of *V*, and $\vec{n}$ the outward drawn normal unit vector.

3 Results and analysis

3.1 Effect of different thickness of binary MEPCM drywall

3.1.1 Temperature profiles of the binary MEPCM drywalls

The internal drywall surface boundary layer, being closest to the outdoor conditions (see Fig.1), responds faster in terms of temperature changes to the outdoor ambient temperature changes and therefore could be used for the analysis of the whole binary MEPCM drywall layer. To this end, the temperature conditions at the internal surface boundary layer of the binary MEPCM drywalls were analysed for both the low and high temperature cycles in order to evaluate the thermal storage behaviour and capacity of the binary MEPCM drywalls. As shown in Fig.3, the period during which the internal drywall boundary layer surface temperature rose was extended from 12 hours to 17 hours for both low and high temperature cycles when the drywall thickness was increased from 1 mm to 5 mm. The charging temperature also dropped into the phase change transition zone from 25.55°C to 23.55°C for the low temperature cycle due to the presence of MEPCM-oct. The similar phenomena could be observed under the high temperature cycle where the charging temperature increased from 34.99°C to 36.99°C for MEPCM-eic.

Meanwhile, the different thicknesses of the binary MEPCM drywalls during charging/discharging processes also affected the maximum/minimum internal drywall

surface boundary layer temperatures as shown in Fig.3. For example, the low and high temperature cycles for the 1 mm drywall were 20-30°C and 30-40°C respectively whereas the temperatures for the 2 mm and 5 mm thick drywalls were reduced by 0.2°C /4.8°C and 1°C /3.4°C for the low and high temperature cycles, respectively. Particularly, the maximum temperature for the 5 mm drywall was only reached at 25.1°C and 36.5°C in low and high temperature cycles and both of them were lower than T_l in Tab.1. This indicates that the 1 mm and 2 mm binary MEPCM drywalls did charge/discharge fully their latent thermal energy within 24 hours whereas some portion of the 5 mm binary MEPCM drywall was still in the solid phase and has enough capacity to absorb the likely amounts of excess heat in the conditions of the study.

3.1.2 Energy storage/discharge profiles of the binary MEPCM drywalls

The heat fluxes through all of the binary MEPCM drywall layers (see Fig.1) were monitored in order to evaluate the thermal energy storage/discharge capacity of those MEPCM layers. As shown in Fig. 4, the duration of the energy storage periods for the 5 mm thick layer did increase by up to about 3 hours under the low temperature cycle and by 4 hours under the high temperature cycle as compared with the 1 mm and 2mm drywalls. Meanwhile, the maximum heat flux in the 5 mm thick drywall also increased from 10.1 W/m^2 to 26.2 W/m^2 and from 10.1 W/m^2 to 19 W/m^2 for the low

and high temperature cycles respectively. Compared with Fig.3, the heat fluxes of the binary MEPCM drywalls in Fig.4 were significantly increased during the phase change period of the two MEPCMs. In addition, the duration of the thermal energy storage charging time was also significantly extended due to the thicker binary MEPCM drywall, and more specifically, the charging time increased from 3.5 to 6 hours when the MEPCM drywall thickness was changed from 1 mm to 5 mm.

Overall, it can be seen that the 5 mm thick layer did not fully discharge its latent heat energy storage capacity over the 24-hour period which is an indication of its longer period of energy storage capability according to the internal drywall surface boundary layer temperature profiles and the external drywall surface boundary layer heat fluxes of the 5 mm drywall in Fig.3 and Fig.4, respectively. For this reason, a 5 mm thick MEPCM layer would be used for modelling the day and night conditions in the next section.

3.2 Performance of binary and other MEPCM drywalls in a model room

3.2.1 Peak and average indoor air temperature profiles

According to the simulation results in Fig. 5, the monthly indoor peak air temperatures for non-PCM wall conditions were higher than the corresponding outdoor environmental air temperatures. However, the indoor peak air temperatures

for various MEPCM drywalls were lower than the outdoor temperatures, especially in the case of the binary MEPCM drywall which achieved the lowest peak indoor air temperature. This shows that by using the latent thermal storage capacity of the MEPCM or the proposed binary MEPCM wallboard in this space the indoor air temperature could be reduced during the hot seasons. In particular, the binary MEPCM drywall was able to reduce the peak indoor air temperature far more than the other drywall materials and more specifically by 2.9 to 6.7°C.

On the other hand, the monthly indoor average air temperatures for various drywalls were even higher than the outdoor environmental air temperature due to mostly the effects of solar radiation, as it is demonstrated in Fig.6. Although there was no significant difference between the monthly average indoor air temperatures and the outdoor environmental temperatures, the binary MEPCM drywall achieved the lowest value. It can therefore be deduced from the results that an integrated MEPCM building would require less energy to achieve an acceptable thermal comfort level.

3.2.2 Zonal indoor temperature distributions

The results for the six-month simulation period (May to October) of 4416 hours (184 days) are presented according to three temperature ranges as summarized in Tab.4. Analysis of the results show that the length of the time within which the temperature

remained between 21°C and 28°C increased by more than 10% with the laminated binary MEPCM drywall system (61%) as compared to the "NO PCM" wall (49%), the MEPCM-Oct drywalls (49%), and the MEPCM-Eic drywall (51%). The results also show that the binary MEPCM drywall has the benefit of satisfying different weather conditions over the longest period of 2703 hours. Furthermore the results do demonstrate similar conclusions as those obtained by Memarian *et al*. (Memarian 2018), Diaconua and Crucerub (Diaconu and Cruceru 2010), Zhu *et al*. (Zhu, Liu et al. 2015, Zhu, Liu et al. 2016) and Jin and Zhang (Jin and Zhang 2011), which did involve the use of double layers of PCMs for energy storage management in buildings.

However, the binary MEPCM drywall did not show the best thermal performance on certain days. For instance, from 28th June to 30th June the MEPCM-Eic drywall achieved the lowest daily peak air temperature and the lowest differential air temperature between day and night as demonstrated in Fig.7. The reason was that the outdoor air temperature during the assessment period was above 27°C, which made the MEPCM-Oct to remain in the liquid phase during that period. On the other hand, the MEPCM-Oct wallboard achieved the best thermal performance from the 6th to 8th of September as shown in Fig. 8 since the range of change of outdoor air temperatures only affected the melting/solidification temperatures of MEPCM-Oct. Overall, the above simulation results proved that the binary MEPCM drywall was able to improve building thermal performance because the two phase change temperatures could

extend the duration of the latent energy storage period.

4 Conclusions

This study was focused on evaluating the thermal performance of a proposed laminated binary MEPCM drywall in a model room located in Hangzhou, China. The Ansys Fluent simulation results demonstrated that the thermal energy charge time and thermal energy charge/discharge amount of the binary MEPCM drywall were significantly increased when the thickness increased from 1 mm to 5 mm. However, the temperature profiles showed that the binary MEPCM drywall was not fully charged when the drywall thickness increased to 5 mm since the maximum temperatures were reduced by 3.4-4.8°C compared with the 1 mm and 2 mm drywalls. This means that the thermal energy storage capacity of the 5 mm thick layer was enough to balance the thermal energy during day and night in the model building.

The ESP-r simulation results showed that the laminated binary MEPCM drywall performed thermally better than the other types of walls over a period of the six months. In comparison with the building without MEPCM, the binary MEPCM drywall did reduce the peak indoor air temperature in summer by 2.9-6.7°C and was able to increase the number of hours during which indoor air temperatures were within the 21-28°C temperature range by about 12% for the selected location. Even

though the evaluation was focussed on Hangzhou city, the study approach could be used as a guide for evaluating the energy saving potential of laminated binary MEPCM drywalls for buildings under different climate regions. Full scale experimental evaluation of thermal and temperature stabilising effects as well as life cycle cost analysis of the proposed laminated binary MEPCM drywall system are therefore recommended.

References

Alam, M., H. Jamil, J. Sanjayan and J. Wilson (2014). "Energy saving potential of phase change materials in major Australian cities." *Energy and Buildings* **78**: 192-201.

Almeida, F., D. Zhang, A. S. Fung and W. H. Leong (2010). Investigation of Multilayered Phase-Change-Material Modeling in ESP-r. International High Performance Buildings Conference**:** 47.

Alva, G., Y. Lin, L. Liu and G. Fang (2017). "Synthesis, characterization and applications of microencapsulated phase change materials in thermal energy storage: A review." *Energy and Buildings* **144**: 276-294.

Ansys (2015). Fluent User's Guide 7.7.2 Specific Heat Capacity as a Function of Temperature.

Ansys (2015). Theory Guide-5.2.1.1 The Energy Equation.

Ansys (2015). Theory Guide-18.4 Energy Equation.

Berardi, U. (2017). "A cross-country comparison of the building energy consumptions and their trends." *Resources, Conservation and Recycling* **123**(Supplement C): 230-241.

Berthou, Y., P. H. Biwole, P. Achard, H. Sallée, M. Tantot-Neirac and F. Jay (2015). "Full scale experimentation on a new translucent passive solar wall combining silica aerogels and phase change materials." *Solar Energy* **115**(0): 733-742.

Darkwa, J., O. Su and T. Zhou (2012). "Development of non-deform micro-encapsulated phase change energy storage tablets." *Applied Energy* **98**: 441-447.

Darkwa, J. and W. Su (2017). "Multiphase-Change Materials for Energy Storage Application in Buildings." *Journal of Thermophysics and Heat Transfer* **31**(4): 791-795.

Darkwa, K. and J. S. Kim (2004). "Heat transfer in neuron composite laminated phase-change drywall." *Proceedings of the Institution of Mechanical Engineers, Part A: Journal of Power and Energy* **218**(2): 83-87.

Diaconu, B. M. and M. Cruceru (2010). "Novel concept of composite phase change material wall system for year-round thermal energy savings." *Energy and Buildings* **42**(10): 1759-1772.

Du, K., J. Calautit, Z. Wang, Y. Wu and H. Liu (2018). "A review of the applications of phase change materials in cooling, heating and power generation in different temperature ranges." *Applied Energy* **220**: 242-273.

ESP-r (2015). Open source building simulation program. **2016**.

Fateh, A., D. Borelli, F. Devia and H. Weinläder (2018). "Summer thermal performances of PCM-integrated insulation layers for light-weight building walls: effect of orientation and melting point temperature." *Thermal Science and Engineering Progress*.

Heim, D. and J. A. Clarke (2004). "Numerical modelling and thermal simulation of PCM–gypsum composites with ESP-r." *Energy and Buildings* **36**(8): 795-805.

Jamekhorshid, A., S. M. Sadrameli, R. Barzin and M. M. Farid (2017). "Composite of wood-plastic and micro-encapsulated phase change material (MEPCM) used for thermal energy storage." *Applied Thermal Engineering* **112**: 82-88.

Jin, X. and X. Zhang (2011). "Thermal analysis of a double layer phase change material floor." *Applied Thermal Engineering* **31**(10): 1576-1581.

Judkoff, R. and J. Neymark (1995). International Energy Agency Building Energy Simulation Test (BESTEST) and Diagnostic Method, National Renewable Energy Laboratory.

Konuklu, Y., M. Ostry, H. O. Paksoy and P. Charvat (2015). "Review on using microencapsulated phase change materials (PCM) in building applications." *Energy and Buildings* **106**(0): 134-155.

Kuznik, F. and J. Virgone (2009). "Experimental assessment of a phase change material for wall building use." *Applied Energy* **86**(10): 2038-2046.

Lee, K. O., M. A. Medina, X. Sun and X. Jin (2018). "Thermal performance of phase change materials

(PCM)-enhanced cellulose insulation in passive solar residential building walls." *Solar Energy* **163**: 113-121.

Memarian, S., B. M. Kari, R. Fayaz and S. Asadi (2018). "Single and combined phase change materials: Their effect on seasonal transition period." *Energy and Buildings* **169**: 453-472.

Mi, X., R. Liu, H. Cui, S. A. Memon, F. Xing and Y. Lo (2016). "Energy and economic analysis of building integrated with PCM in different cities of China." *Applied Energy* **175**: 324-336.

Su, W., J. Darkwa and G. Kokogiannakis (2015). "Review of solid–liquid phase change materials and their encapsulation technologies." *Renewable and Sustainable Energy Reviews* **48**(0): 373-391.

Su, W., J. Darkwa and G. Kokogiannakis (2017). "Development of microencapsulated phase change material for solar thermal energy storage." *Applied Thermal Engineering* **112**: 1205-1212.

Su, W., J. Darkwa and G. Kokogiannakis (2018). "Nanosilicon dioxide hydrosol as surfactant for preparation of microencapsulated phase change materials for thermal energy storage in buildings." *International Journal of Low-Carbon Technologies* **13**(4): 301-310.

Su, W., J. Darkwa, G. Kokogiannakis, T. Zhou and Y. Li (2017). "Preparation of microencapsulated phase change materials (MEPCM) for thermal energy storage." *Energy Procedia* **121**: 95-101.

Su, W., T. Zhou, Y. Li and Y. Lv (2019). "Development of microencapsulated phase change material with poly (methyl methacrylate) shell for thermal energy storage." *Energy Procedia* **158**: 4483-4488.

Thiele, A. M., A. Jamet, G. Sant and L. Pilon (2015). "Annual energy analysis of concrete containing phase change materials for building envelopes." *Energy Conversion and Management* **103**: 374-386.

Tokuç, A., T. Başaran and S. C. Yesügey (2015). "An experimental and numerical investigation on the use of phase change materials in building elements: The case of a flat roof in Istanbul." *Energy and Buildings* **102**: 91-104.

Yi, J. (2005). China Standard Weather Data for Analyzing Building Thermal Conditions. Beijing, China Building Industry Publishing House.

Young, B. A., G. Falzone, Z. Wei, G. Sant and L. Pilon (2018). "Reduced-scale experiments to evaluate performance of composite building envelopes containing phase change materials." *Construction and Building Materials* **162**: 584-595.

Zhou, T., J. Darkwa and G. Kokogiannakis (2015). "Thermal evaluation of laminated composite phase change material gypsum board under dynamic conditions." *Renewable Energy* **78**: 448-456.

Zhu, N., F. Liu, P. Liu, P. Hu and M. Wu (2016). "Energy saving potential of a novel phase change

material wallboard in typical climate regions of China." *Energy and Buildings* **128**: 360-369.

Zhu, N., P. Liu, P. Hu, F. Liu and Z. Jiang (2015). "Modeling and simulation on the performance of a novel double shape-stabilized phase change materials wallboard." *Energy and Buildings* **107**: 181-190.

Table 1: Thermophysical properties of the two MEPCM layers

Name	ρ(kg/m^3)	Cp (J/kg°C)	k (W/mK)	T_m (°C)	T_l (°C)	L (kJ/kg)
MEPCM-oct	658	2202	0.154	23.55	25.55	179
MEPCM-eic	684	2115	0.166	34.99	36.99	194

Table 2: Physical properties of wall in the studied lightweight building

Item	Layers	Material	Thickness (mm)	k (W/mK)	ρ (kg/m^3)	Cp (J/kgK)	IR emission	Solar absorption factor
Wall	1	Wood	9	0.14	530	900	0.1	0.1
	2	Fiberglass	66	0.04	12	840		
	3	Plaster board	12	0.16	950	840	0.1	0.1

Table 3: Physical properties of floor, door and window in lightweight building

Item	Layers	Material	Thickness (mm)	k (W/mK)	ρ (kg/m^3)	Cp (J/kgK)	IR emission	Solar absorption factor
Roof	1	Wood	19	0.14	530	900	0.1	0.1
	2	Fiberglass	111.8	0.04	12	840		
	3	Plaster board	10	0.16	950	840	0.1	0.1
Floor	1	Floor insulation	1003	0.04	10	100	0.9	0.9
	2	Timber floor	25	0.14	650	1200	0.9	0.6
Door	1	Wood	15	0.51	1400	1000	0.9	0.6
Window	1	Glass	3.2	1.06	2500	750	0.1	0.1
	2	Air gap	13	0	0	0		
	3	Glass	3	1.06	2500	750	0.9	0.1

Table 4: Indoor temperature distributions

Indoor Air temperature ranges	NO PCM		MEPCM-Oct		Binary MEPCM		MEPCM-Eic	
	Time (h)	Time (%)	Time (h)	Time (%)	Time (h)	Time (%)	Time (h)	Time (%)
T<21°C	916	21%	864	20%	589	13%	720	16%
21°C≤T≤28°C	2155	49%	2174	49%	2703	61%	2258	51%
T>28°C	1345	30%	1378	31%	1124	25%	1439	33%
Total time	4416 hours, 100%							

Figure Captions

Figure 1: Physical model of laminated binary MEPCM drywall

Figure 2: Physical model of the lightweight building

Figure 3: Internal surface temperature profiles of the binary MEPCM drywall with different thicknesses from the Fluent simulations

Figure 4: External surface heat flux profiles of the binary MEPCM drywalls with different thicknesses from the Fluent simulations

Figure 5: Monthly peak air temperature profiles by ESP-r

Figure 6: Monthly average air temperature profiles by ESP-r

Figure 7: Indoor and outdoor air temperature profiles for 28-30 June from ESP-r simulations

Figure 8: Indoor and outdoor air temperature profiles for 6-8 September from ESP-r simulations

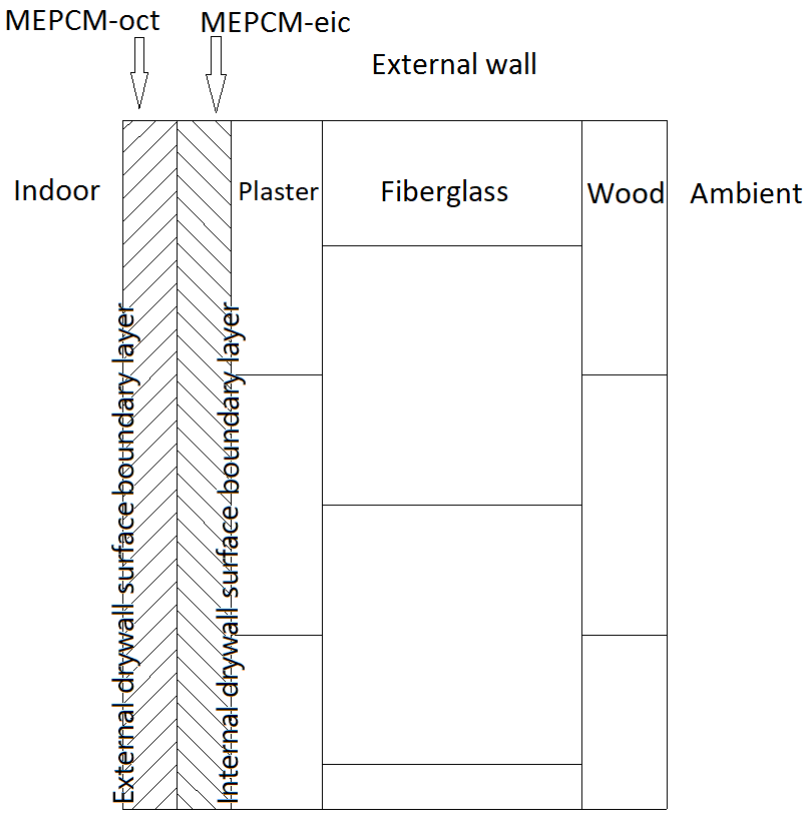

Figure 1: Physical model of laminated binary MEPCM drywall

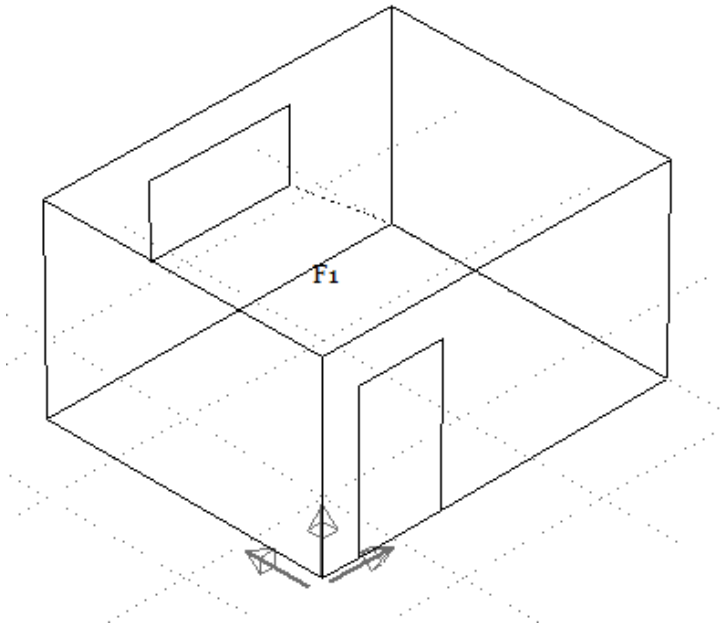

Figure 2: Physical model of the lightweight building

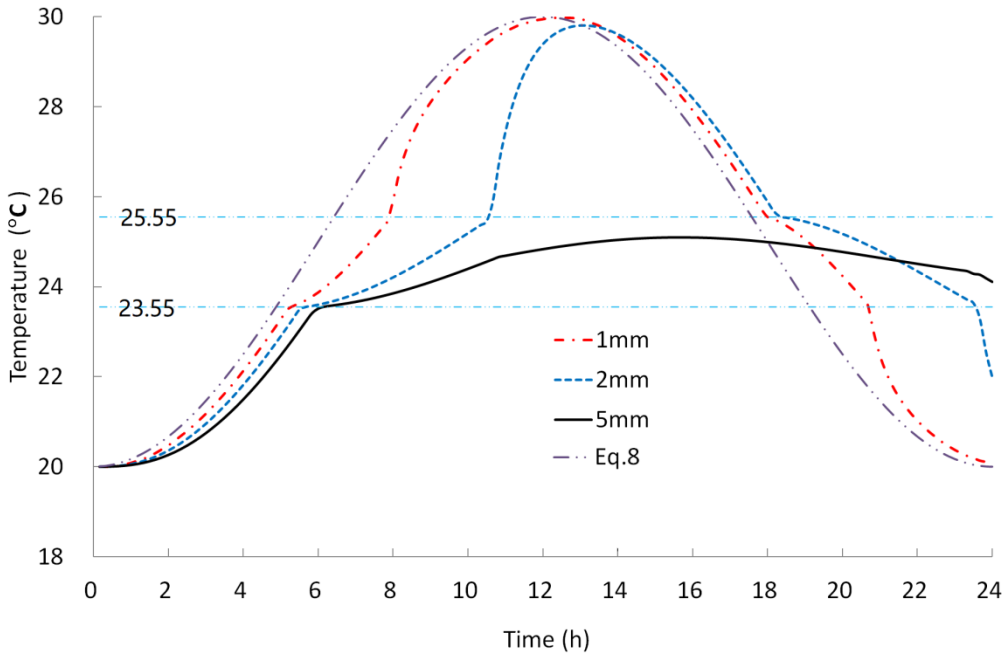

(a) Low temperature cycle

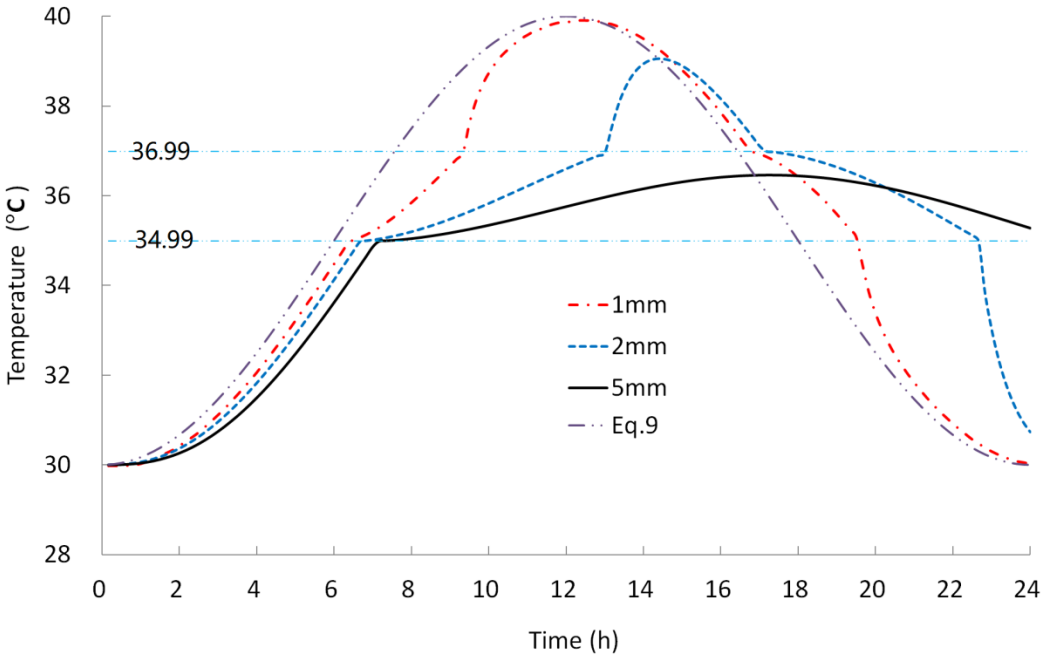

(b) High temperature cycle

Figure 3: Internal surface temperature profiles of the binary MEPCM drywall with different thicknesses from the Fluent simulations

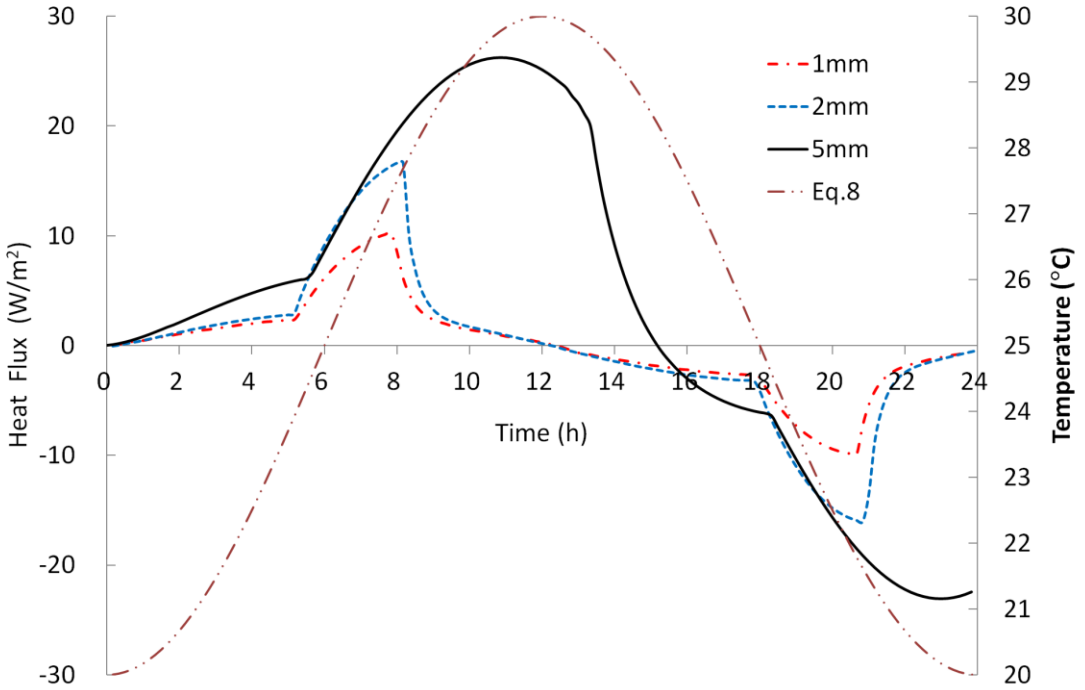

(a) Low temperature cycle

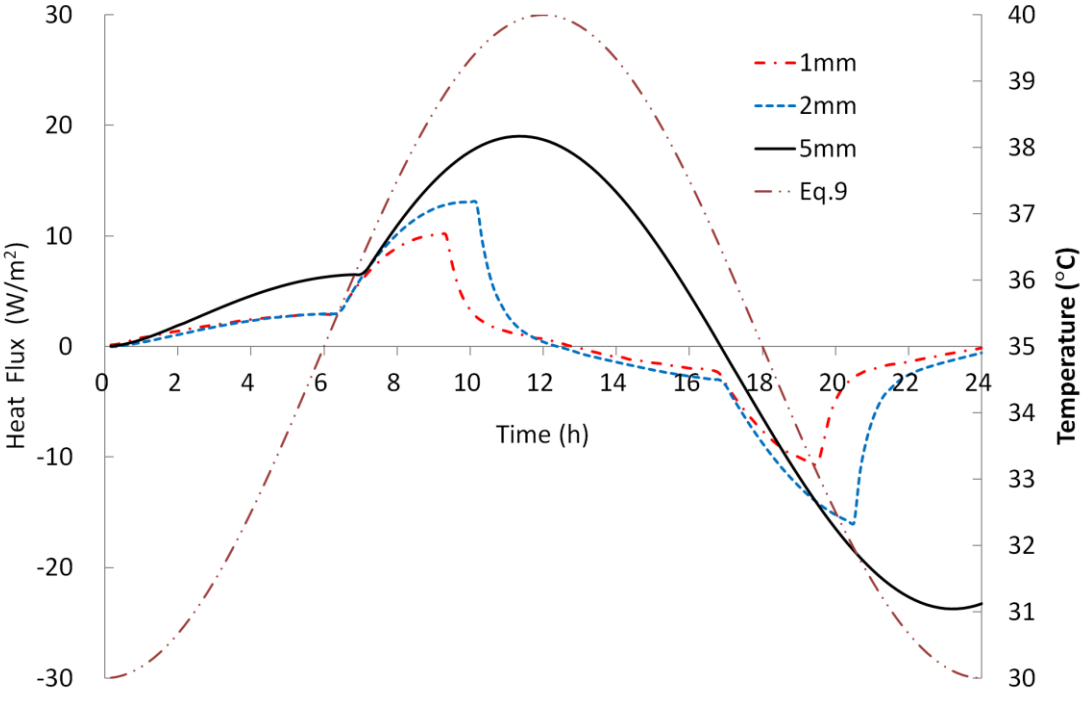

(b) High temperature cycle

Figure 4: External surface heat flux profiles of the binary MEPCM drywalls with different thicknesses from the Fluent simulations

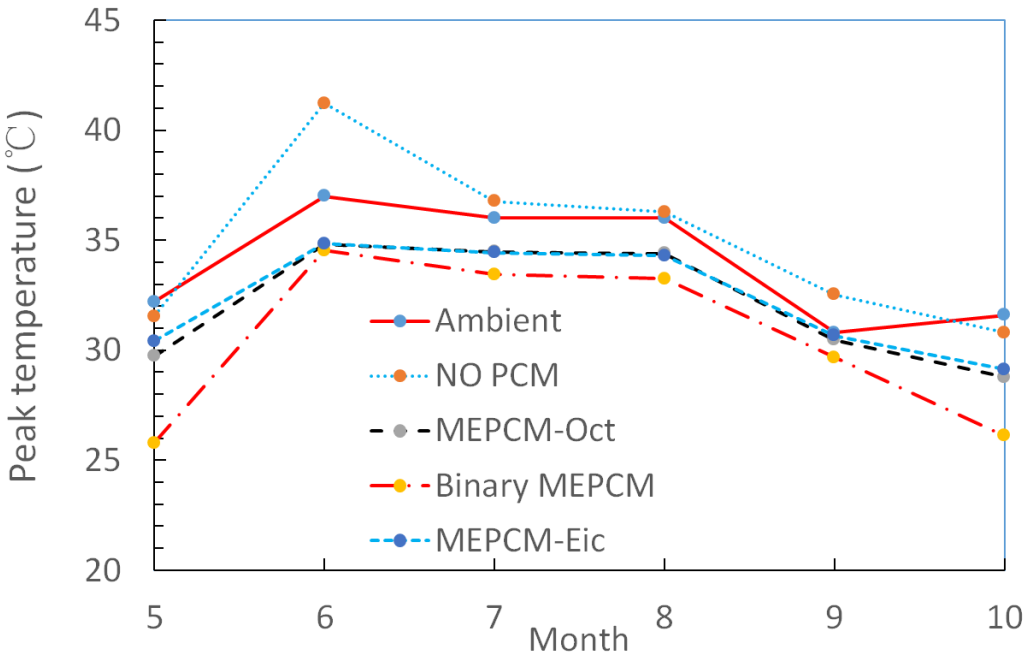

Figure 5: Monthly peak air temperature profiles by ESP-r

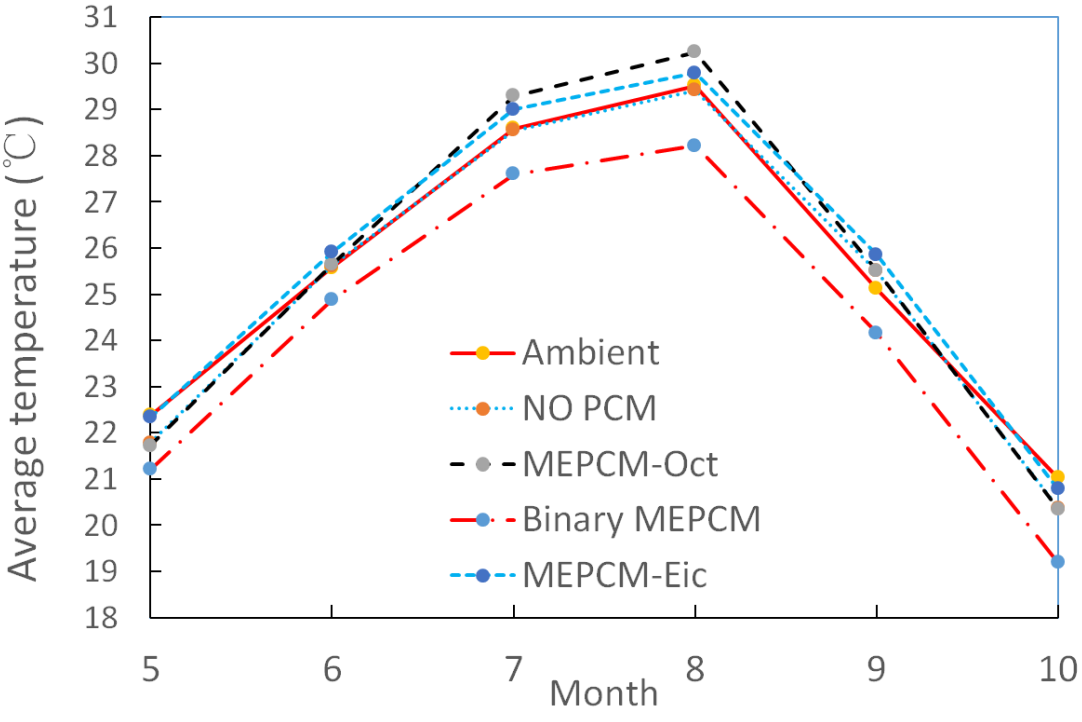

Figure 6: Monthly average air temperature profiles by ESP-r

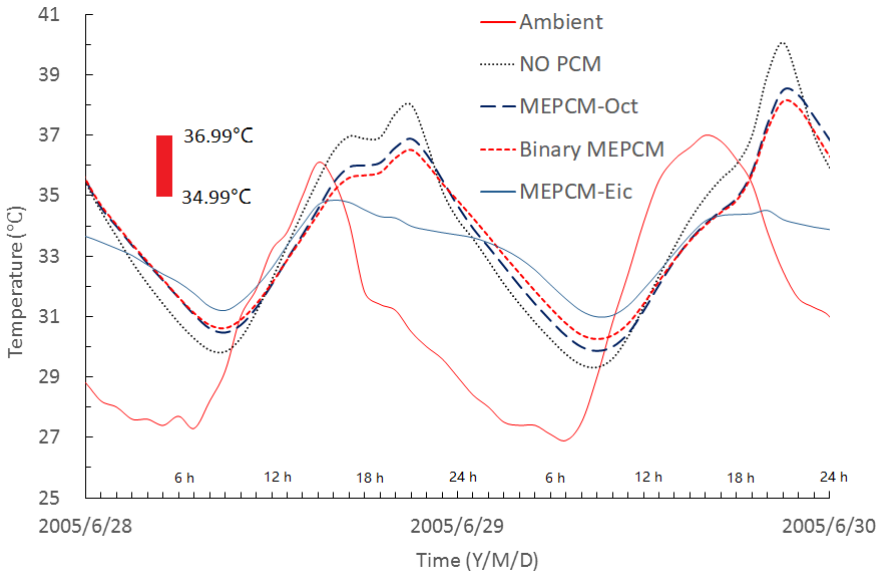

Figure 7: Indoor and outdoor air temperature profiles for 28-30 June from ESP-r simulations

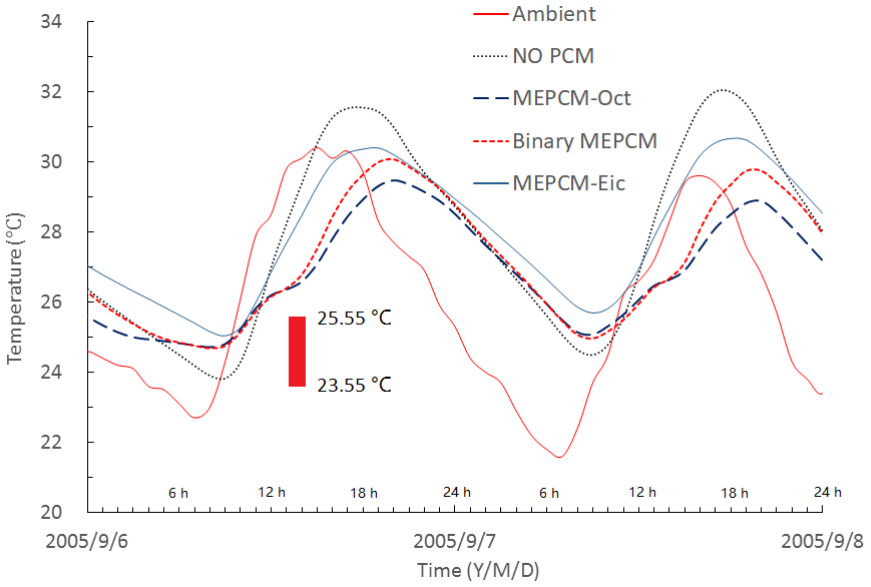

Figure 8: Indoor and outdoor air temperature profiles for 6-8 September from ESP-r simulations